Monitoring of implanted stem cell migration *in vivo*: A highly resolved *in vivo* magnetic resonance imaging investigation of experimental stroke in rat

Mathias Hoehn[†‡§], Ekkehard Küstermann[†‡], James Blunk[†], Dirk Wiedermann[†], Thorsten Trapp[†], Stefan Wecker[†], Melanie Föcking[†], Heinz Arnold[†], Jürgen Hescheler[¶], Bernd K. Fleischmann[¶], Wolfram Schwindt[†], and Christian Bührle[†]

[†]Max Planck Institute for Neurological Research, Gleuelerstrasse 50, D-50931 Cologne, Germany; and [¶]Department of Neurophysiology, University of Cologne, D-50937 Cologne, Germany

Edited by Louis Sokoloff, National Institutes of Health, Bethesda, MD, and approved October 7, 2002 (received for review July 23, 2002)

In vivo **monitoring of stem cells after grafting is essential for a better understanding of their migrational dynamics and differentiation processes and of their regeneration potential. Migration of endogenous or grafted stem cells and neurons has been described in vertebrate brain, both under normal conditions from the subventricular zone along the rostral migratory stream and under pathophysiological conditions, such as degeneration or focal cerebral ischemia. Those studies, however, relied on invasive analysis of brain sections in combination with appropriate staining techniques. Here, we demonstrate the observation of cell migration under *in vivo* conditions, allowing the monitoring of the cell dynamics within individual animals, and for a prolonged time. Embryonic stem (ES) cells, constitutively expressing the GFP, were labeled by a lipofection procedure with a MRI contrast agent and implanted into rat brains. Focal cerebral ischemia had been induced 2 weeks before implantation of ES cells into the healthy, contralateral hemisphere. MRI at 78-μm isotropic spatial resolution permitted the observation of the implanted cells with high contrast against the host tissue, and was confirmed by GFP registration. During 3 weeks, cells migrated along the corpus callosum to the ventricular walls, and massively populated the borderzone of the damaged brain tissue on the hemisphere opposite to the implantation sites. Our results indicate that ES cells have high migrational dynamics, targeted to the cerebral lesion area. The imaging approach is ideally suited for the noninvasive observation of cell migration, engraftment, and morphological differentiation at high spatial and temporal resolution.**

embryonic stem cells | cerebral ischemia | cell labeling

Several studies have been able to demonstrate the migrational capacity of endogenous stem or progenitor cells in rat and mouse brains during normal (1, 2) and pathophysiological conditions (3, 4). The therapeutical potential of stem cell grafting has recently been studied in various pathological conditions of the brain showing extensive cell migration after implantation. However, all investigations so far have required the invasive analysis of brain sections postmortem in various groups of animals for different survival periods. A recent investigation described the detection of labeled cells, injected into rats, but reported no specific cell migration in the *in vivo* MRI data (5). All other studies have investigated the potential of MRI to detect pretreated cells (5–7) by registering the MRI data *ex vivo*, thus permitting observation of only one time point. In the present investigation we demonstrate sufficient spatial and temporal resolution of experimental MRI at high fields to allow longitudinal studies on individual animals after stem cell implantation into the brain. We have investigated the spatial dynamics of implanted embryonic stem (ES) cells and demonstrated their high migrational potential from the implantation site in the normal brain hemisphere toward the ischemic lesion in the opposite hemisphere, showing their massive population of the ischemic borderzone 3 weeks after implantation and 5 weeks after induction of focal cerebral ischemia.

Materials and Methods

Animal Model. All experiments were performed in accordance with the National Institutes of Health animal protection guidelines and approved by local governmental authorities.

All surgical procedures were performed on spontaneously breathing male Wistar rats (body weight, 260–300 g), anesthetized with 1% halothane in 3:7 (vol/vol) O_2/N_2O. Temporary occlusion of the right middle cerebral artery for 60 min was performed on 11 animals by the intraluminal thread occlusion technique as described (8, 9). Retraction of the endovascular suture allowed successful reperfusion to the territory supplied by the middle cerebral artery. After middle cerebral artery occlusion, animals were allowed to recover from anesthesia and, under close control, were placed in their cages in the animal facility. For comparison, three healthy rats served as control group, receiving only implantation of ES cells.

Two weeks after transient cerebral ischemia, animals underwent implantation surgery. During the MRI session directly after implantation, and during repetitive scans over 3 weeks, the spontaneously breathing animals were anesthetized with 0.6–0.8% halothane in O_2/N_2O. Depth of anesthesia was monitored by breathing excursions of the thorax wall, visualized by placing of a water-filled latex bulb, connected to a transducer, under the chest of the animal. During the whole magnetic resonance experiment, body temperature was measured with a rectal thermocouple and kept constant at 37°C with a feedback-controlled warm-water blanket.

Implantation. Two depots of ES cells of 30,000 cells each were grafted into the border between the cortex and the corpus callosum (0.5 mm anterior, 3.0 mm lateral to bregma, 2.0 mm ventral from the dural surface), and, respectively, into the striatum (0.5 mm anterior, 3.0 mm lateral to bregma, 5.0 mm ventral from the dural surface) of the left intact hemisphere, contralateral to the ischemic territory. The normal hemisphere (instead of the ischemic borderzone) was chosen for the implantation sites because an environment supportive for the implanted cells was preferred. Such an environment was not assumed to exist in the ischemic borderzone, which itself struggles for survival.

For implantation surgery, animals were fixed spontaneously breathing under halothane anesthesia in a stereotactic frame. Homogeneous single cell suspensions in DMEM were delivered

This paper was submitted directly (Track II) to the PNAS office.

Abbreviations: ES, embryonic stem; USPIO, ultra-small superparamagnetic iron-oxide particles.

[‡]M.H. and E.K. contributed equally to this work.

[§]To whom correspondence should be addressed. E-mail: mathias@mpin-koeln.mpg.de.

to the implantation site through a minute glass capillary (outer diameter, 80 μm) attached to a Hamilton syringe and a micropump system.

Cell Culture and Lipofection. HT22 cells (10) were grown in DMEM supplemented with 5% FCS and penicillin-streptomycin (stock solution 1:100). Murine ES cells of the D3 cell line, stably transfected with the pCX-(β-act)-enhanced GFP expression vector as described (11), were cultivated in DMEM containing 15% FCS, nonessential amino acids (stock solution 1:100), penicillin-streptomycin (stock solution 1:100), 50 μM β-mercaptoethanol and leukemia inhibitory factor (100 nM).

Labeling of the cells was achieved with the magnetic resonance contrast agent SINEREM (generous gift of C. Corot, Guerbet, France) consisting of ultrasmall superparamagnetic iron-oxide particles (USPIO). For this purpose, the lipofection technique, generally used for the infusion of DNA into cell nuclei, was applied by using the lipofection reagent FuGENE. Coincubation of FuGENE and SINEREM in serum-free DMEM for 30 min led to the encapsulation of the contrast agent by FuGENE, consequently facilitating the contrast agent infusion into the cells. The required concentration conditions included incubation of the cells with FuGENE (1 μl/ml) and SINEREM (2–14 mg/ml = 400–2,800 μg Fe/ml) for 24 h in the corresponding medium. Labeling efficiency of the cells with the contrast agent by this lipofection procedure was estimated to be better than 70%. After harvesting cells were washed several times, diluted, and injected immediately.

MRI. All experiments were performed on an experimental animal scanner at 7T (Bruker BioSpec; Bruker, Billerica, MA) equipped with actively shielded gradient sets of 200 mT/m. For rf irradiation and signal detection custom-built coils were used. A 12-cm-diameter Helmholtz coil arrangement served for rf excitation, whereas signal detection was achieved with a 23-mm-diameter surface coil. The coils were decoupled from each other.

Imaging was achieved with either a 2D multislice or a 3D FLASH sequence. The 2D sequence used a slice thickness of 500–700 μm and an inplane resolution of 50 μm. With the 3D sequence, a matrix of 256 $\times$ 160 $\times$ 128 was recorded; after zero-filling and Fourier transformation this resulted in a 256 $\times$ 256 $\times$ 128 matrix. Selection of a field of view of 20 $\times$ 12 $\times$ 10 mm^3 lead to a spatial pixel resolution of 78 $\times$ 49 $\times$ 78 μm^3, equivalent to 0.3 nl. With TR/TE 200 ms/20 ms and a flip angle of 20–25°, this required an experimental time of 1.1 h per complete 3D data set.

Immunohistochemistry. Immunohistochemistry was performed in cryostat sections that were air-dried and fixed in ethanol/acetone (1:1 vol/vol). Slides were incubated for 24 h at 4°C with a polyclonal GFP antibody (1:100; Santa Cruz Biotechnology) in PBS containing 5% normal goat serum and 0.3% Triton X-100. Thereafter, sections were washed and incubated with a biotinylated goat anti-rabbit antibody (1:150; Dako). After washing streptavidin-horseradish peroxidase (VECTASTAIN Elite ABC; Vector Laboratories) was added and immunoreactivity was visualized by detection of the biotin-streptavidin-peroxidase complex by incubation with 0.5 mg/ml diaminobenzidine tetrahydrochloride in PBS and 0.05% hydrogen peroxide.

Results

Spatial Resolution of Cell-Specific MRI Contrast. To examine the sensitivity of the MRI technique, we performed *in vitro* titrations of labeled cells. Neurons of a murine hippocampal cell line, HT-22 cells (10), were labeled with SINEREM by lipofection and injected in an agarose gel mimicking the MRI signal behavior of brain tissue. Based on these experiments, cell clusters as small as maximally 40 cells still led to an MRI contrast sufficient to allow reliable detection against the background.

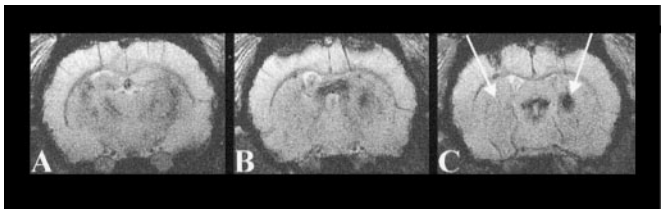

Fig. 1. Coronal multislice gradient-echo magnetic resonance images through a rat brain after stereotactical implantation of HT-22 neuronal cells into the striatum of both hemispheres. On the right hemisphere HT-22 cells were labeled with SINEREM by lipofection, whereas on the left hemisphere implanted cells remained native (see arrows). Note the strong signal decrease at the implantation location of the labeled cells on the right hemisphere. The volume of labeled cells is distinguished mainly in the two posterior contiguous image planes (mainly *B* and *C*). The hyperintensity in the upper mid-left region of the brain, just ventral of the corpus callosum, is caused by the high water content of the lateral ventricle.

To test the sensitivity of this approach under *in vivo* conditions, labeled cells were implanted into one hemisphere whereas unlabeled, native cells were implanted into the other hemisphere within the striatum of Wistar rats. Native, unlabeled cells produced no contrast in the rat brain and remained undetectable in the image, whereas labeled cells were readily observed within scan times of only a few minutes (Fig. 1). Under these *in vivo* conditions, the sensitivity of the method was demonstrated to permit detection of as few as ≈500 cells directly after implantation (data not shown).

Transgenic ES cells, derived from a mouse cell line (11), were labeled by the same lipofection procedure: cells were incubated with 8.8 mg/ml SINEREM (= 1.76 mg Fe/ml) together with FuGENE, resulting in a high-efficiency (better than 70%) lipofection of the cells with the contrast agent. This labeling concentration led to highly saturated conditions in the cells, thus leaving MRI contrast conditions unaltered in *in vitro* proliferation studies during up to 10 cell cycles (E.K., unpublished data). When implanted into host brain tissue, this labeling led to a strong susceptibility change with severe signal damping in strongly T_2*-weighted MRI (Fig. 2). It thus produces a strong contrast against the normal tissue background. Spatial resolution of the imaging modality, being largely determined by sensitivity of rf-detector components and strength of space encoding magnetic field gradients, at present is routinely at a 3D isotropic

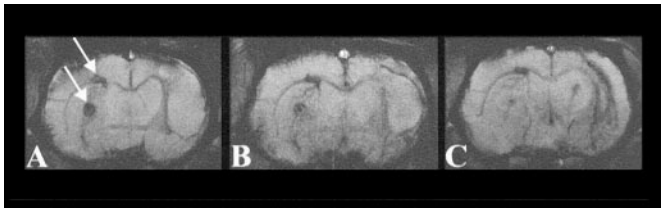

Fig. 2. Coronal sections from a 2D multislice MRI experiment through a rat brain at the day of stem cell implantation (*A*) and 8 days (*B*) and 16 days (*C*) after implantation. Transient focal cerebral ischemia of the right hemisphere (60 min) had been induced 14 days before implantation. Note the two large circular dark tissue areas (*A*, arrows) demonstrating the location of the labeled stem cells, on the strongly T_2*-weighted images with the contrast produced by the USPIO-based contrast agent SINEREM in the ES cells. The cortical implantation area extends toward the subventricular zone by 8 days after implantation. By 16 days, the lesioned hemisphere, opposite to the hemisphere of implantation, shows an extended darkened area at the striatum, reflecting the massive accumulation of ES cells in the lesion periphery. In plane resolution, 50 $\times$ 50 μm^2; slice thickness, 500 μm.

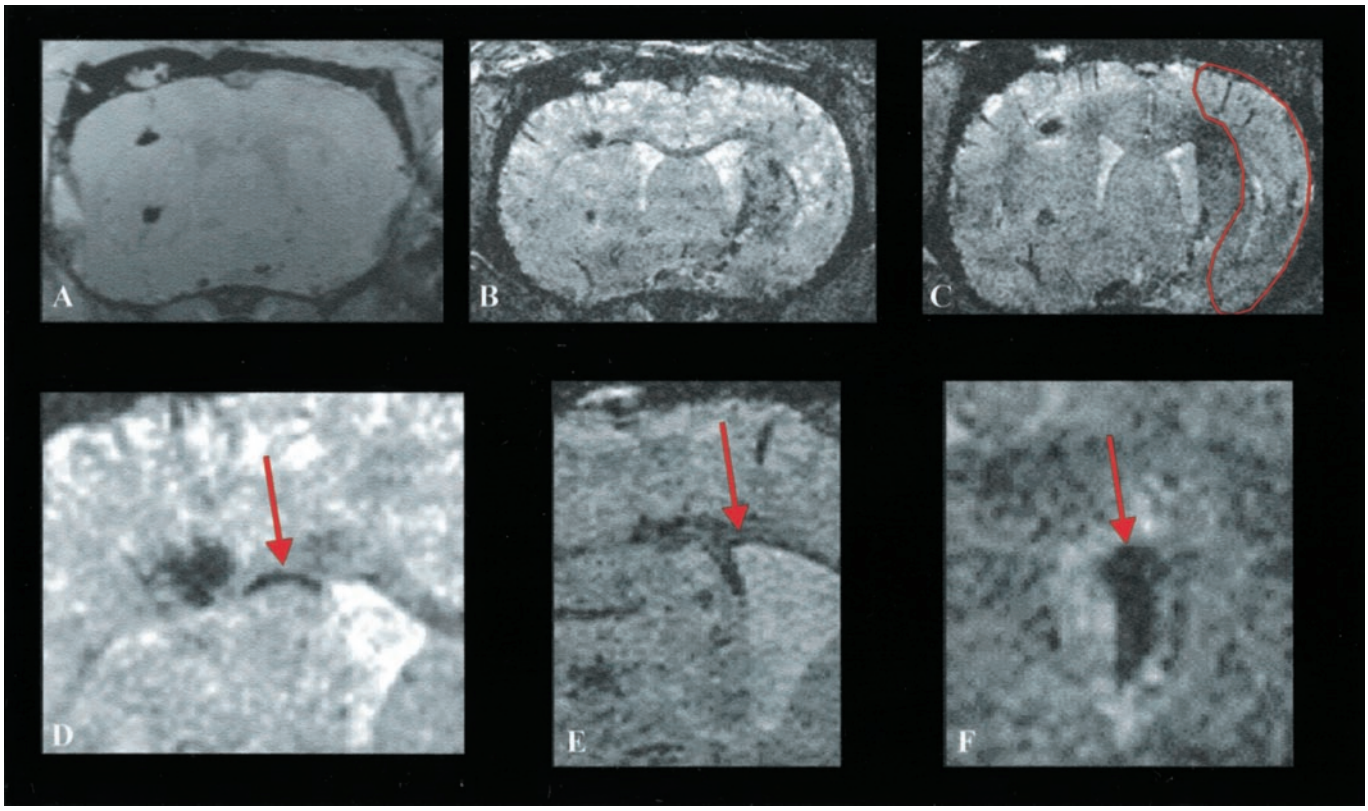

Fig. 3. Coronal section through a rat brain at various times after implantation of ES cells into the hemisphere contralateral to the induced transient 60-min focal ischemia. 3D data sets were recorded at the day of implantation (*A*) and at 6 (*B*) and 8 (*C*) days after implantation. For orientation, the necrotic tissue area is outlined on *C*. Note at 6 days (*B*) the discrete dark line (arrow in *D*, with higher magnification) along the corpus callosum between the cortical implantation site and the ventricular wall showing cells migrating toward the lesioned hemisphere. At 8 days (*C*) a dark region becomes visible in the dorsal part of the lesioned territory reflecting first arrival of USPIO-labeled cells. At higher magnification (*D*), the migration along the corpus callosum becomes more pronounced and is clearly visible. Taken from another animal example, the lining along the ventricular wall (*E*) and the accumulation of labeled stem cells on the choroid plexus (*F*) are also presented with high magnification.

resolution of 78 μm producing a signal-to-noise ratio of 8–10 within approximately 1 h experimental time.

Assessment of Tolerance to Labeling Procedure. To assess the tolerance of the ES cells to the paramagnetic label, toxicity studies were performed in the cell culture. Cells were labeled with increasing concentrations of SINEREM between 2 and 14 mg/ml (=400–2,800 μg Fe/ml). Dead cells were stained with trypan blue at 24 h, counted under the microscope, and expressed as percent of total cells per field-of-view segment. For comparison, the staurosporin toxicity assay was included. The number of dead cells was ≈2–3%, independent of labeling concentration within the tested range, and was indistinguishable from unlabeled control cultures. For the hippocampal cell line HT-22, the fraction of dead cells was even below 1% for all SINEREM concentrations. Further, comparing *in vitro* proliferation of labeled and unlabeled cell cultures with the aim of determining proliferation-dependent label dilution, no clear differences in proliferation intensity was observed (E.K., unpublished data). Finally, support for vitality of labeled cells comes from their contrast behavior after implantation. To investigate the contrast under condition of lysed cells releasing the contrast agent into the extracellular space, free SINEREM was injected into the striatum, which led to rapidly dissipating MRI contrast with the contrast agent diffusing radially from the injection site through the extracellular space (data not shown). Such a dynamic contrast pattern was not observed after implantation of labeled cells, supporting the notion that the cells are vital after implantation.

ES Cell Implantation After Stroke. To examine whether ischemic lesions will induce migrational activity, 60-min transient focal cerebral ischemia was induced in Wistar rats by using the established intraluminal thread technique (8, 9). This ischemia resulted in severe damage of the ipsilateral hemisphere with necrobiotic or necrotic tissue areas in the middle cerebral artery-supplying territory, encompassing both the cortex and the lateral part of the striatum. Two weeks after ischemia induction, ES cells were labeled with SINEREM and ≈30,000 cells were stereotactically implanted both into the cortex (next to the corpus callosum) and into the striatum of the normal contralateral hemisphere. Directly after implantation, the sites were visible as circular dark tissue areas (Fig. 2*A*). Within a few days, thin dark, strongly contrasted lines became visible within the corpus callosum (Fig. 2*B*), medial to the implantation site, showing stem cells in migration toward the lesioned opposite hemisphere. In another animal and with 3D data sets (Fig. 3 *B* and *D*) such thin lines were differentiated in even more detail and were analyzed as a 3D blanket of cells within the corpus callosum migrating away from the primary implantation site. Many of the cells apparently gathered near the subventricular zone (Fig. 3*E*), giving a strong contrast. As a general finding in the group of animals, this cell accumulation extended over time to produce a lining effect of the ventricular wall. Furthermore, in most animals accumulation of labeled ES cells was observed on the choroid plexus of the lateral ventricle in the ischemic hemisphere (Fig. 3*F*).

Within days after implantation, in all ischemic animals, an

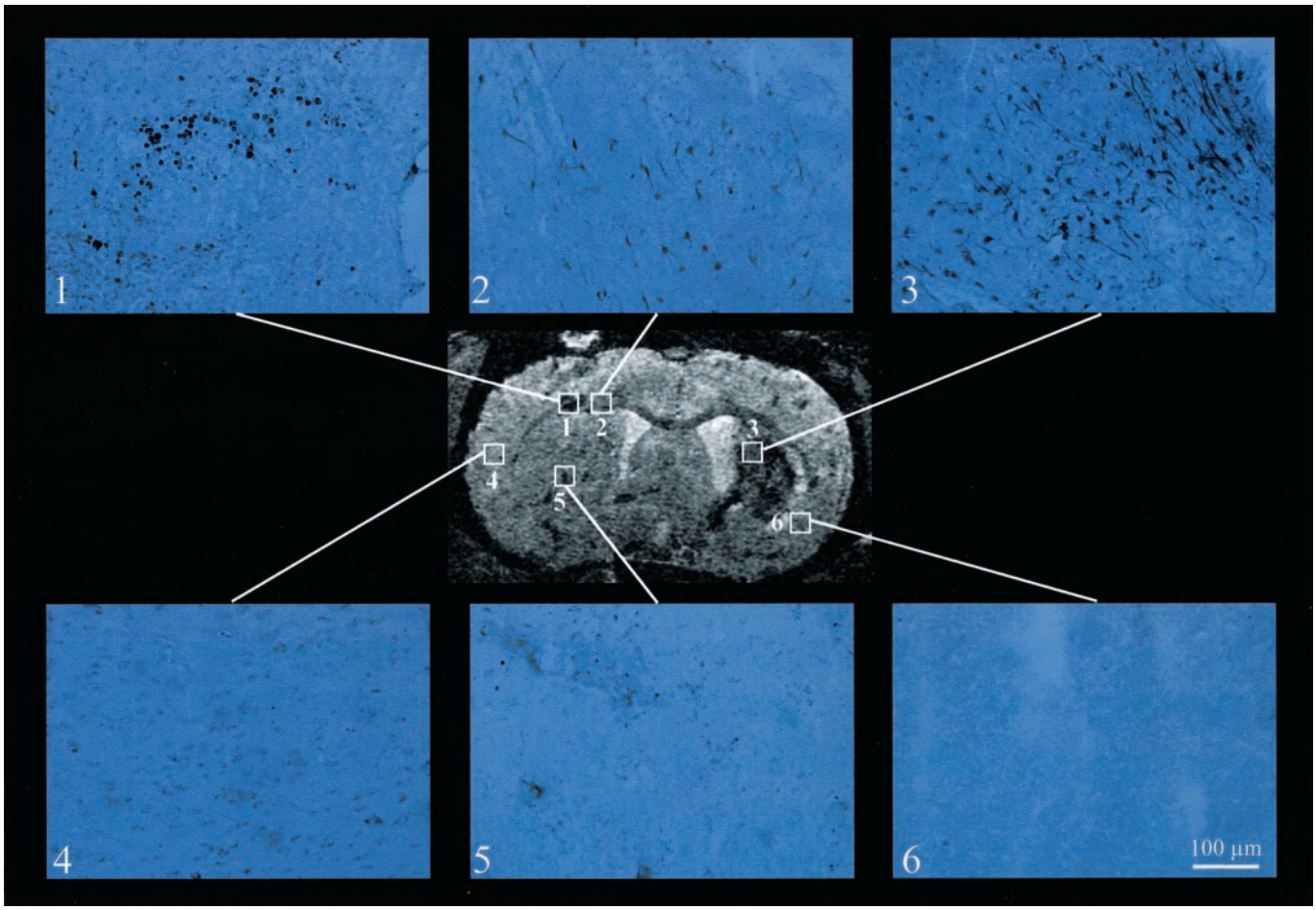

Fig. 4. Several locations have been marked on a section from a 3D data set at 11 days after implantation (same experiment as Fig. 3). For these positions GFP immunohistochemistry is shown. Clearly, in the primary implantation sites (sites 1 and 5), in the corpus callosum (site 2), and in the periphery of the ischemic lesion (site 3) strong staining shows the presence of GFP-expressing ES cells. Note that although the cell morphology shows round shapes at the implantation sites (sites 1 and 5), ES cells become elongated already during their migration (site 2). On arrival in the lesioned hemisphere several of the cells show neuron-like shapes of cell body with long dendritic- or axon-like extensions. In the necrotic area (of the formerly ischemic core) (site 6) no GFP-expressing cells have shown up, in agreement with the lack of USPIO-induced contrast in the T_2*-weighted image. Spatial resolution of the 3D MRI experiment: $78 \times 78 \times 78\ \mu m^3$. Microscopy of the immunohistochemically stained section used a primary magnification of $\times 400$ for all plates. (Scale bar for sites 1–6 = 100 μm.)

increasing contrast was observed on the ischemic hemisphere, beginning at the dorsal end of the striatum adjacent to the corpus callosum (Fig. 3*B*). From there, it rapidly spread during the next few days to extend across the striatum and parts of the lateral cortex by 2 weeks after implantation (Figs. 2*C*, 3*C*, and 4).

In contrast to these findings of pronounced migration in stroke-induced animals, no signal change beyond the primary implantation site was noted in three healthy animals, implanted with ES cells by using the identical implantation protocol. The MRI data were unchanged during an observation period of up to 20 days after implantation.

Colocalization of MRI Contrast and GFP Immunohistochemistry. To examine the nature of this developing contrast in the ischemic borderzone, correlation with independent means to detect the implanted stem cells was assessed. For this purpose, the intrinsic fluorescence of the constitutive GFP expression of the ES cells was studied. In parallel, immunohistochemistry was performed with an antibody against GFP in coronal brain sections, corresponding to the planes of the MRI investigation. GFP-induced fluorescence was observed very weakly in the vicinity of the primary implantation site, but was strong around the ventricular wall facing the cortical implantation site. In the ischemic hemisphere, fluorescence was registered dispersed across large regions in the ischemic territory, close to necrotic tissue areas (data not shown). GFP immunohistochemistry demonstrated few cells close to the implantation canal and extended cell clusters within the corpus callosum. Massive infiltration of GFP-active cells was detected in the ischemic territory in proximity to necrotic tissue areas (Fig. 4). This finding convincingly demonstrated the migration of ES cells across the corpus callosum into the lesioned tissue. As visible on the immunohistochemically stained sections (Fig. 4), the cells change their morphology from purely globular at the implantation site to more differentiated shapes within the corpus callosum, and with an appearance of neuronal differentiation with long-extended dendrite- and axon-like shapes in the ischemic target area.

Discussion

Methodological Aspects. A recent investigation described the detection of labeled cells, injected into rats, but reported no specific cell migration in the *in vivo* MRI data (5). Other studies have investigated the potential of MRI to detect pretreated cells (5–7) by registering the MRI data *ex vivo*, thus permitting observation of only one time point. The present study demonstrates the sufficient sensitivity and spatial resolution to detect,

under true *in vivo* conditions,[‖] migration of discrete clusters of cells implanted in host tissue. From our *in vitro* titration studies and from *in vivo* variation of cell numbers, we estimate that some of these cell clusters, detectable under our conditions, are smaller than 100 cells. This increased sensitivity is explained by an interaction of several factors. First of all, the here described lipofection procedure of labeling the cells in culture with an MRI contrast agent has proved to result in very high efficiency of cell loading with the used dextran-coated iron oxide nanoparticles of SINEREM.[**††]

Several other approaches labeling cells for MRI detection have been reported in the literature. Some strategies are limited to the intrinsically high-contrast agent uptake of T cells and macrophages (12–14), others in their pioneering works have produced transgenic cells expressing, for example, the transferrin receptor and thus being susceptible to the uptake of conjugates of transferrin and monocrystalline iron oxide nanoparticles (15, 16). Again, other approaches required the complex formation between contrast agent and the transactivator protein (Tat) of HIV-1 (17, 18). Our own present labeling procedure is simple and robust; it is based on commercially available components without requiring the complex chemical synthesis of custom-tailored intracellular contrast agents (5), thus making our labeling strategy readily available for other application laboratories. Electron microscopy experiments of labeled stem cell cultures (K.-A. Hossmann, personal communication) show that the cells, treated with our lipofection procedure, are rich in lysosomes containing a large number of electron-dense spots representing the crystalline iron-oxide core of the SINEREM particles. Because no electron-dense particles were found in the cytosol, it is concluded that the deposition of the iron-oxide particles within lysosomes is a sequestration process isolating the contrast agent from the cytosol, thus explaining the nonexistent acute toxicity of the labeling procedure.

A few reports (5–7) had implanted magnetically labeled cells into nervous tissues, but then detection by MRI was achieved only on excised tissue specimen *ex vivo* (6, 7), and by using also extremely long measurement times of many hours (6) to achieve the necessary signal-to-noise ratio and the contrast. In other cases, the spatial resolution was kept so low that no detail about localization or even movement of the implanted cells could be discerned (5). Here, we succeeded in demonstrating spatial resolution of isotropic 78 μm.[‡‡] This has been achieved through an integrated technical approach combining the high magnetic field strength of a 7 Tesla experimental animal scanner for improved sensitivity with custom-tailored special rf-hardware developments, building dedicated rf detection coils.[§§] It should be pointed out here that the USPIO-based high contrast is achieved quite as well already at low magnetic fields. The high-field system in our case, however, results in higher signal-to-noise ratio per unit time thereby significantly reducing necessary experimental scan time for the sensitive detection of small cell volumes. In fact, by using similar strategies other groups have been successful in improving the spatial resolution even down to 1 μm for their special application of imaging thin plant stems (19). For imaging macroscopic animal species, however, where a dedicated animal horizontal bore scanner is needed, we have reported on spatial resolution down to 30 μm (20), a situation that in principle may be transferred to our present investigation. This would then bring the contrast resolution in the vicinity of the detection of individual labeled cells in the host tissue.

For longitudinal studies, animals are usually weakened because of the induced cerebral lesion. Therefore, the repetitive MRI sessions have to be kept short so that the animals will tolerate the periods of anesthesia. In our present investigation, the high-resolution magnetic resonance images are achieved within an experimental time frame of about 1–2 h which is fully compatible with the required short (repetitive) periods of anesthesia.

Biological Aspects. We have observed pronounced spatial dynamics of the implanted stem cells within short periods. During the period of a few days only, the dynamics of the labeled cells showed a clear directional, very pronounced migration toward the lesion on the hemisphere opposite to the primary implantation sites. Because of this long distance between the implantation site and the lesion, the directed cell mobility is interpreted as a strong, long-range chemotactic signal being present, with a concentration gradient radial from the lesion. Such a chemotactic gradient would then explain the attraction of the implanted stem cells toward the lesion target. Existence and origin of such a signal are presently not understood. However, we speculate that an up-regulation and expression of growth factors within the lesion or at the lesion borderzone may play a role in this process. The neurotrophin family consists of neuronal growth factor, brain-derived neurotrophic factor, and neurotrophins, of which neuronal growth factor has been shown to be up-regulated within the first 6 h after the onset of the ischemic lesion (21) but is down-regulated again shortly after that. Brain-derived neurotrophic factor regulates the differentiation, survival, and maintenance of developing and adult neurons (22). Brief episodes of ischemia have been shown to lead to a dramatic overexpression of the mRNA level of brain-derived neurotrophic factor (23). After kainate lesioning, a long-lasting trophic response was reported, correlated with a specific overexpression of brain-derived neurotrophic factor that is maintained for at least six months (24).

Further, the described migrational mobility of the cells must depend on the interaction between the particular, implanted cells and the host tissue. This interaction will most likely involve the extracellular matrix as well as cell adhesion molecules on the membrane surface of the migrating cells.

Our GFP immunohistochemical data provide morphological evidence that indicates differentiation of the implanted stem cells beginning already shortly after having migrated away from the primary implantation site. At least, such morphological changes from globular cell shapes to pronounced elongation are noted when the cells are detected in the corpus callosum. On arrival in the target zone, the ischemic periphery on the opposite hemisphere, a majority of the GFP active cells (implanted stem cells) is positive of neuronal staining by NeuN (C.B., unpublished data), but also many astrocytes and some oligodendrocytes are found in the ischemic penumbra. This fact that the cells begin to change from the original, fully undifferentiated stem cell status to various degrees of differentiation indicates the presence of a signal triggering this differentiation process. However, at present, origin, identity, and way of interaction of this signal are unknown.

[‖]Wiedermann, D., Küstermann, E., Blunk, J., Wecker, S., Bührle, C., Schwindt, W., Trapp, T., Föcking, M., Hescheler, J. & Hoehn, M., Proceedings of the Tenth Annual Scientific Meeting of the International Society for Magnetic Resonance in Medicine, May 18–24, 2002, Honolulu, p. 1257 (abstr.).

**Küstermann, E., Wiedermann, D., Bührle, C., Arnold, H., Föcking, M., Trapp, T. & Hoehn, M., Proceedings of the Tenth Annual Scientific Meeting of the International Society for Magnetic Resonance in Medicine, May 18–24, 2002, Honolulu, p. 1255 (abstr.).

††Frank, J. A., Zywicke, H., Miller, B., Arbab, A. S., Jordan, E. K., Lewis, B. K., Bryant, L. H. & Bulte, J. W. M., Proceedings of the Tenth Annual Scientific Meeting of the International Society for Magnetic Resonance in Medicine, May 18–24, 2002, Honolulu, p. 391 (abstr.).

‡‡Küstermann, E., Trapp, T., Blunk, J., Wiedermann, D., Bührle, C., Wecker, S., Föcking, M., Schwindt, W., Hescheler, J. & Hoehn, M., Proceedings of the Tenth Annual Scientific Meeting of the International Society for Magnetic Resonance in Medicine, May 18–24, 2002, Honolulu, p. 713 (abstr.).

§§Wecker, S., Küstermann, E., Rademacher, B. & Hoehn, M., Proceedings of the Tenth Annual Scientific Meeting of the International Society for Magnetic Resonance in Medicine, May 18–24, 2002, Honolulu, p. 878 (abstr.).

Therapeutical Aspects. The focus of the present investigation lies on the detectability assessment and observation of implanted stem cells under *in vivo* conditions in the intact animal. Therefore, the survival periods were limited to 3–4 weeks after stem cell implantation (i.e., 5–6 weeks after the ischemic insult). At this early time, meaningful assessment of outcome improvement by the chosen therapeutical approach cannot be expected. However, the present data point to the highly interesting potential for therapeutical strategies concerning regenerative medicine, aimed at tissue regeneration, that is, repair. The reported migrational cell activity clearly indicates that the cerebral lesion triggers a signal leading to an intensive interaction between the implanted cells and the host tissue. Although this signal is most likely originally meant for endogenous mechanisms (e.g., activation of adult stem cells in the subventricular zone or the granular cell layer), it induces a massive accumulation of stem cells in the lesion periphery and, at the same time, triggers a pronounced differentiation process. Once these mechanisms are better understood, their application offers the potential for an active influence of migrational and directional mobility, providing an active means for guiding cells toward preferential target zones. At the same time, these mechanisms will help directing the fate of preferential differentiation. Thus, a strategy aiming at regenerative medicine may in the future take advantage of these host tissue–cell interaction mechanisms to guide cells to their target and select the cell type most needed for the restoration of a functional neuronal network.

In summary, the present investigation demonstrates the sensitivity for the detection of small clusters of labeled cells in the rat brain tissue by using MRI at ultra-high spatial resolution, within experimental times acceptable for *in vivo* investigations, even tolerable for animals with weakened physiological condition because of their disease state. Furthermore, the present methodological approach shows *in vivo* observation of cell engraftment, migration, and morphological changes within the brain after implantation. The method opens a variety of fields for the study of the biology of stem cells under *in vivo* conditions, an aspect of particular interest for the investigation of the therapeutical potential of cellular replacement strategies.

We are grateful to Dr. Claire Corot (Guerbet, France) for the generous gift of SINEREM. The support by grants from the Deutsche Forschungsgemeinschaft (SFB194,B1), the German Federal Ministry of Education and Research Bundesministerium für Bildung und Forschung (Kompetenznetzwerk Schlaganfall, B5), and the binational research program (German–Israeli-Program Deutsch-Israelisches Program) is gratefully acknowledged.

1. Lois, C. & Alvarez-Buylla, A. (1994) *Science* **264,** 1145–1148.
2. Lois, C., Garcia-Verdugo, J.-M. & Alvarez-Buylla, A. (1996) *Science* **271,** 978–981.
3. Magavi, S. S., Leavitt, B. R. & Macklis, J. D. (2000) *Nature* **405,** 951–955.
4. Veizovic, T., Beech, J. S., Stroemer, R. P., Watson, W. P. & Hodges, H. (2001) *Stroke* **32,** 1012–1019.
5. Bulte, J. W. M., Douglas, T., Witwer, B., Zhang, S.-C., Strable, E., Lewis, B. K., Zywicke, H., Miller, B., van Gelderen, P., Moskowitz, B. M., *et al.* (2001) *Nat. Biotechnol.* **19,** 1141–1147.
6. Bulte, J. W. M., Zhang, S.-C., van Gelderen, P., Herynek, V., Jordan, E. K., Duncan, I. D. & Frank, J. A. (1999) *Proc. Natl. Acad. Sci. USA* **96,** 15256–15261.
7. Franklin, R. J. M., Blaschuk, K. L., Bearchell, M. C., Prestoz, L. L., Setzu, A., Brindle, K. M. & Ffrench-Constant, C. (1999) *NeuroReport* **10,** 3961–3965.
8. Kohno, K., Back, T., Hoehn-Berlage, M. & Hossmann, K.-A. (1995) *Magn. Reson. Imaging* **13,** 65–71.
9. Olah, L., Wecker, S. & Hoehn, M. (2001) *J. Cereb. Blood Flow Metab.* **21,** 430–439.
10. Li, Y., Maher, P. & Schubert, D. (1997) *Neuron* **19,** 453–463.
11. Kolossov, E., Fleischmann, B. K., Liu, Q., Bloch, W., Viatchenko-Karpinski, S., Manzke, O., Ji, G. J., Bohlen, H., Addicks, K. & Hescheler, J. (1998) *J. Cell Biol.* **143,** 2045–2056.
12. Yeh, T. C., Zhang, W., Illstad, S. T. & Ho, C. (1993) *Magn. Reson. Med.* **30,** 617–625.
13. Yeh, T. C., Zhang, W., Illstad, S. T. & Ho, C. (1995) *Magn. Reson. Med.* **33,** 200–208.
14. Moore, A., Weissleder, R. & Bogdanov, A., Jr. (1997) *J. Magn. Reson. Imaging* **7,** 1140–1145.
15. Weissleder, R., Moore, A., Mahmood, U., Bhorade, R., Benveniste, H., Chiocca, E. A. & Basilion, J. P. (2000) *Nat. Med.* **6,** 351–354.
16. Moore, A., L., Josephson, L., Bhorade, R. M., Basilion, J. P. & Weissleder, R. (2001) *Radiology* **221,** 244–250.
17. Lewin, M., Carlesso, N., Tung, C.-H., Tang, X.-W., Cory, D., Scadden, D. T. & Weissleder, R. (2000) *Nat. Biotechnol.* **18,** 410–414.
18. Dodd, C. H., Hsu, H. C., Chu, J. W., Yang, P., Zhang, H. G., Mountz, J. D., Jr., Zinn, K., Forder, J., Josephson, L., Weissleder, R., *et al.* (2001) *J. Immunol. Methods* **256,** 89–105.
19. Lee, S.-C., Kim, K., Kim, J., Lee, S., Yi, J. H., Kim, S. W., Ha, K.-S. & Cheong, C. (2001) *J. Magn. Reson.* **150,** 207–213.
20. Wecker, S., Hörnschemeyer, T. & Hoehn, M. (2002) *Magn. Reson. Imaging* **20,** 105–111.
21. Guégan, C., Ceballos-Picot, I., Nicole, A., Kato, H., Onténiente, B. & Sola, B. (1998) *Exp. Neurol.* **154,** 371–380.
22. Lewin, G. R. & Barde, Y. A. (1996) *Annu. Rev. Neurosci.* **19,** 289–317.
23. Lindvall, O., Ernfors, P., Bengzon, J., Kokaia, Z., Smith, M.-L., Siesjö, B. K. & Persson, H. (1992) *Proc. Natl. Acad. Sci. USA* **89,** 648–652.
24. Suzuki, F., Junier, M.-P., Guilhem, D., Sorensen, J.-C. & Onténiente, B. (1995) *Neuroscience* **64,** 665–674.